Polystyrene-*block*-polyisoprene Nanofiber Fractions. 1. Preparation and Static Light-Scattering Study

Guojun Liu* and Xiaohu Yan

Department of Chemistry, University of Calgary, 2500 University Dr., NW, Calgary, Alberta, T2N 1N4, Canada

Scott Duncan

Defense Research Development Canada−Suffield, PO Box 4000 Station Main, Medicine Hat, Alberta, T1A 8K6, Canada

Received July 1, 2002; Revised Manuscript Received October 22, 2002

ABSTRACT: Block copolymer nanofibers may be viewed as the macroscopic counterparts of polymer chains or supra−polymer chains. Well-characterized nanofiber fractions with narrow length distributions are required to facilitate their study by techniques such as viscometry and dynamic light scattering. Polystyrene-*block*-polyisoprene (PS-*b*-PI) nanofibers were prepared in this study by stirring S_2Cl_2-treated PS-*b*-PI films in THF to separate and disperse the cross-linked PI cylindrical domains. Nanofiber fractions were obtained by combining centrifugation fractionation and ultrasonication. These fractions were characterized by transmission electron microscopy to obtain their length distribution functions and static light scattering to yield the weight-average molar masses and *z*-average radii of gyration. A quantitative analysis of the radius of gyration values revealed that the PS-*b*-PI nanofibers had a persistence length of ∼200 nm in THF.

I. Introduction

Block copolymer nanofibers (BCNs) can be prepared from either cylindrical micelles[1−3] formed in a block-selective solvent or block-segregated copolymer solids.[4] Nanofibers are obtained in a block-selective solvent via the direct cross-linking of the core block of the cylindrical micelles.[5,6] In bulk, block copolymers self-assemble forming various intricate nanometer-sized block segregation patterns. At a volume fraction of ∼30%, the minority block of a diblock normally forms hexagonally packed cylinders dispersed in the continuous matrix of the majority block.[4] Nanofibers are obtained by cross-linking the minority block and separating the hairy cylinders via solvent dispersion.[7−10] In this paper we report on the preparation of nanofibers from polystyrene-*block*-polyisoprene or PS-*b*-PI, where PI acts as the minority or cross-linking block.

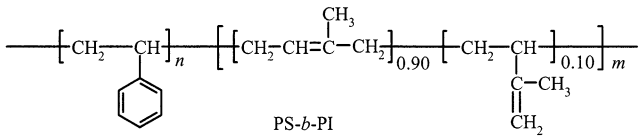

PS-*b*-PI

As mentioned recently,[11] BCNs may be viewed as the macroscopic counterparts of polymer chains or supra−polymer chains. Illustrated in Scheme 1 is the structural comparison between a poly(*n*-hexyl isocyanate), PHIC, chain, and a PS-*b*-PI nanofiber.

In a PHIC chain, the backbone is made of imide units joined linearly, and the hairs are $-(CH_2)_5CH_3$. Their counterparts in a PS-*b*-PI nanofiber would be the cross-linked PI cylinder and PS chains, respectively. It remained to be seen if such fibers would have solution properties[12] similar to those of polymer chains. To check this, one would need well-characterized nanofiber fractions of different lengths. Thus, in this paper, we also report on the preparation of nanofiber fractions of varying lengths and their characterization by transmission electron microscopy (TEM) and static light scattering (SLS).

Scheme 1. Structural Comparison between a PS-*b*-PI Nanofiber (Left) and a PHIC Chain (Right) at Different Magnifications

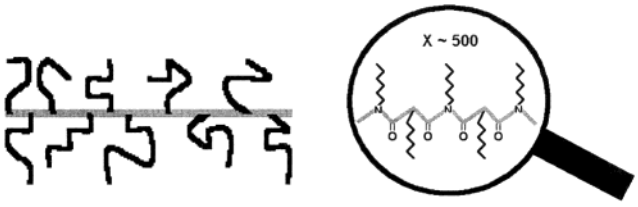

Nanofibers obtained from the diblock solid-state synthesis method are typically tens of micrometers long and polydisperse in length. Techniques such as light scattering, traditionally used for polymer study, cannot be employed to characterize such fibers. We obtained a nanofiber fraction with a relatively narrow length distribution by separating it first from the longer fibers by centrifugation at 11 000*g* and then from the shorter fibers by centrifugation at 18 000*g*. This fraction, fraction 1 or F1, was then ultrasonicated for different times to yield F2, F3, F4, and F5, with even shorter lengths. TEM was used to obtain the average lengths and length distribution functions, $N(L)$, for the fractions. SLS was used to obtain the weight-average molar masses M_w and the *z*-average radii of gyration R_G. Combining the $N(L)$ and R_G data, we also calculated the persistence length, l_p, for each fraction.

There have been many reports on cylindrical micelle studies.[13] However, owing to the structural instability or "living" nature[14] of the cylindrical micelles, one could neither fractionate the micelles nor study the fractions. It is our hope that studies of BCNs will shed light on the long-standing and complex issue of cylindrical micelle characterization. The use of BCNs will help to

10.1021/ma021021b CCC: $22.00
Published on Web 11/21/2002

Table 1. Characteristics of PS and PS-*b*-PI, Where PS Is the Precursor Block to the Diblock

polymer	$\bar{M}_n$ (g/mol) GPC	$\bar{M}_w/\bar{M}_n$ GPC	*n*/*m* NMR	1,4-content NMR (%)	*n*	*m*
PS	23 000	1.04			220	
PS-*b*-PI	31 000	1.07	1.60	90	220	140

extend the study of synthetic polymers to unprecedented length scales.

II. Experimental Section

Diblock Copolymer. The PS-*b*-PI sample used was purchased from Polymer Source, Inc. The characteristics of the PS precursor and the diblock are shown in Table 1. The PS block consisted of 220 units as determined from size exclusion chromatography. Using this *n* value and the *n*/*m* ratio of 1.60 as determined from NMR, we obtained $m = 140$. Both the PS block and the diblock had low polydispersity. The high 1,4-content of 90% for the PI block was attributed to the use of cyclohexane as the polymerization medium.[15]

PS-*b*-PI Film Formation and Cross-Linking. The diblock, 1.00 g, was dissolved in toluene bubbled with argon to yield a ~15 wt % solution. The solution was cast in a Petri dish with a diameter of 15 cm and placed in a vacuum desiccator. The solvent was evaporated under the protection of N_2 over 4−5 days. The dried diblock film was then exposed to S_2Cl_2 (Aldrich, 98%) vapor for 1 week to cross-link the PI cylindrical domains. By the end of the experiment, there was an excess of S_2Cl_2 liquid condensed on the diblock film surface.

Nanofiber Preparation. The cross-linked PS-*b*-PI films were first evacuated under reduced pressure to remove the excess S_2Cl_2 condensed on the film surfaces or sorbed inside the polymer matrix. It was then stirred in THF for 1 week to disperse most of the cross-linked cylinders. The nanofibers were separated from the gel by centrifugation at 1000*g*. The supernatant was then added to methanol to precipitate the nanofibers.

The nanofiber precipitate was redispersed into THF. Longer fibers were further separated from the shorter fibers by centrifugation at 11 000*g*. A fraction, F1, with relatively narrow molar mass distribution was obtained after separating it from the even shorter fibers by centrifugation at 18 000*g*. We could not get further fractions by centrifugation fractionation as 18 000*g* approached the upper acceleration limit of our centrifuge. Fractions 2, 3, 4, and 5 were obtained alternatively by ultrasonicating fraction 1 with a Branson model 1200 R−C (voltage equals 117 V, and current equals 1.3 A) ultrasonicator for 1, 2, 8, and 16 h, respectively.

Light-Scattering Studies. Nanofibers at a concentration of $\sim 5 \times 10^{-6}$ g/mL were dispensed in a vial with a special lid. The lid contained a gas inlet that was fitted with a 0.1 μm filter and an outlet that was fitted with a polyethylene tube. After the vial was centrifuged at 1100*g* for 30 min, it was carefully taken out of the centrifuge and secured in a clamp. Pressure was applied through a syringe connected to the filter to push out the nanofiber solution via the polyethylene tube that was suspended halfway into the nanofiber solution. After the initial portion was discarded, the middle fraction was dispensed into a clean cylindrical quartz cell with a diameter of 2.5 cm for light scattering measurements. A total of 19 scattering angles were used in each measurement with the lowest angle set at 12°. The angle increment used was 1° for F1 and F2, 1.5° for F3 and F4, and 2° for F5. To ensure data precision, light intensities at each concentration were measured once in a low to high angle scan and another time in a high to low angle scan and the intensities in the two scans at each angle were then averaged. The light scattering instrument used was a Brookhaven model BI-200SM. Each sample was analyzed by light scattering at least twice, and the deviation between the two runs was typically less than ±3%.

The difference, Δn_r, between the refractive index of the PS-*b*-PI nanofiber solutions and that of THF, the solvent, was determined using a differential refractometer (Precision Instruments Co.) with light that had passed a band-pass filter centered around 633 nm. Plotting $\Delta n_r/c$ vs *c*, where *c* denotes nanofiber concentration, yielded a straight line with an intercept or the specific refractive index dn_r/dc of 0.171 mL/g.

Table 2. Elemental Analysis Results for Nanofibers Produced in Different Layers of a PS-*b*-PI Film

sample	% C	% H
top layer	64.35	5.43
	63.78	5.83
	63.66	5.85
middle layer	63.83	5.85
bottom layer	64.43	5.89

Transmission Electron Microscopy Study. Transmission electron microscopy (TEM) was used to obtain the length distributions of the nanofiber fractions and to estimate the diameter of the PI cylinders in the PS matrix. To obtain the TEM images of the nanofibers, the fiber dispersions in THF were aspirated on to carbon-coated copper grids using a homebuilt device.[16] The fibers were then stained with OsO_4 vapor for 4 h before viewing by a Hitachi-700 electron microscope operated at 75 kV. Thin sections of the PS-*b*-PI solid were obtained from cryo-microtoming using a Leica Ultracut UCT system (Type 706201, Austria) and were also stained with OsO_4 vapor before viewing by TEM.

III. Results and Discussion

PI Cross-Linking. The PI cylindrical domains were cross-linked via the following reaction:[17]

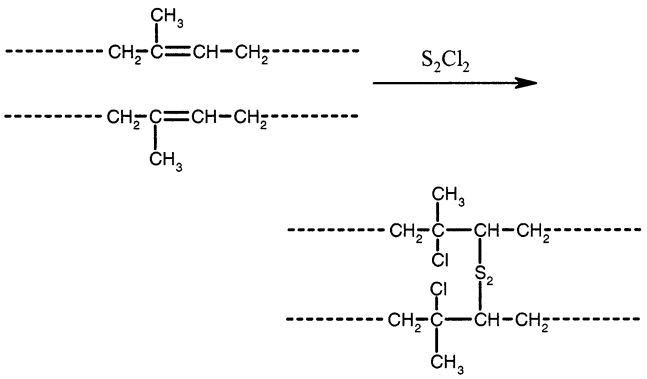

The vapor phase transfer of S_2Cl_2 to the PS-*b*-PI film, as described in the Experimental Section, ensured that S_2Cl_2 was introduced to the reaction sites only gradually to minimize the possibility of the partial reaction of S_2Cl_2. By the end of the treatment, however, the film had been exposed to a considerable excess of S_2Cl_2 to ensure the uniform cross-linking of PI across the whole film thickness. An insufficient amount of S_2Cl_2 would have caused preferential cross-linking of the surface layers of the diblock films. A large excess of S_2Cl_2, if introduced in one aliquot, would have caused the partial reaction of S_2Cl_2 to yield some unreacted S−Cl groups, which could subsequently react, once exposed to the atmosphere, with water to produce thiol groups. To check the success of this strategy, we prepared a film that was ~5 mm thick. After cross-linking the polymer using the above method, we then removed the excess S_2Cl_2 by evacuation. The film was cut parallel to its surface into three layers of approximately equal thickness. The films were then dispersed in THF to yield nanofibers. The nanofibers were purified by precipitation into methanol. Shown in Table 2 are the elemental analysis results for the nanofibers prepared from the film samples taken from the three different layers. The invariance, within

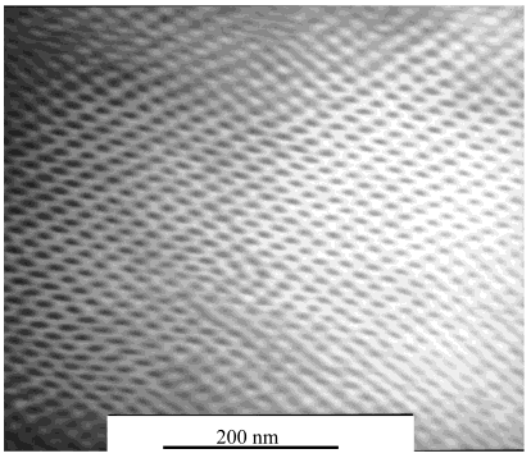

Figure 1. TEM image of a thin section of the PS-*b*-PI solid sample after staining with OsO_4.

experimental error, in composition with layer depth suggests uniform PI cross-linking across the film thickness.

Since the reaction between S_2Cl_2 and PI did not introduce any new carbon atoms, the average carbon content in the final cross-linked sample from the five runs with results shown in Table 2 was readily used to calculate the amount of S_2Cl_2 reacted with PI. This calculation yielded a molar ratio of 0.485 to 1.00 between S_2Cl_2 and the isoprene unit. This value is very close to the theoretical limit of $^1/_2$ and confirms a high degree of PI cross-linking in the nanofiber samples. A quantitative infrared absorption analysis of the double bonds before and after cross-linking showed that the double bond conversion was 90%. Combining these two numbers, we estimated that 86% of the reacted S_2Cl_2 participated in the "bridging" reaction with both chlorine atoms added to PI.

Nanofiber Diameter. A parameter that is of critical importance in the discussion of nanofiber solution intrinsic viscosity, diffusion coefficient, scattering structural factor, and the radius of gyration is the diameter of the nanofibers. We will estimate this value here to facilitate later discussions.

As mentioned above, the nanofibers were prepared from dispersing the cross-linked PI cylinders in THF. Shown in Figure 1 is a TEM image of a thin section of a PS-*b*-PI film. The PI cylinders, which are approximately perpendicular to the image plane, look dark here because the staining agent OsO_4 reacted selectively with the PI domains. The apparent leftward slant is probably due to stress-induced sample deformation during microtoming.

Despite their orientation, the cylinders seem to have the expected hexagonal packing in the relatively lighter region of the TEM image. The measurement of intercylinder distances L_{cic} along the three major symmetry axes of a hexagon yielded an average value 20.3 nm. The L_{cic} value, which could be determined with the highest accuracy relative to other dimension parameters, was then used to yield a calculated diameter d_{PI} of 12.1 nm for the PI cylinders.[18,19] In this calculation, the volume fraction of PI, ϕ_{PI}, was assumed to be 0.32 based on $n/m = 1.60$ and the PI and PS densities of 0.90 and 1.05 g/mL,[20] respectively.

The volume fractions of PS and PI and d_{PI} were also used to calculate the diameter, d, of a dry nanofiber including the PS shell. This calculation yielded $d = 21.4$ nm. Using the d_{PI}, d, and density values, we further calculated the molar mass for "un-cross-linked" nanofibers of unit length to be 1.98×10^5 g/(mol·nm). On the basis of the S_2Cl_2 to isoprene molar ratio of 0.485/1.00 determined for the cross-linked nanofibers, the molar mass for cross-linked nanofibers of unit length was calculated to be 2.53×10^5 g/(mol·nm).

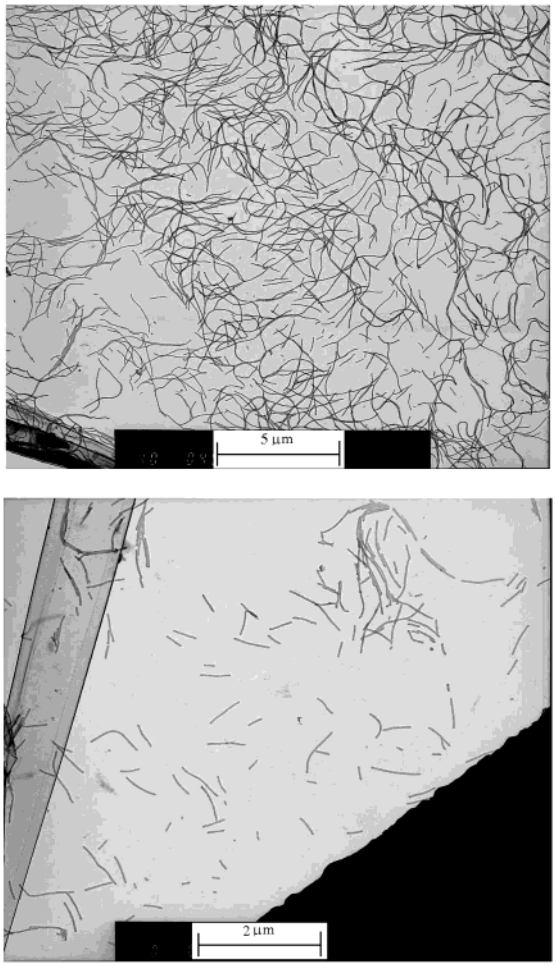

Figure 2. TEM images of PS-*b*-PI nanofiber fraction 1 (a) and fraction 4 (b), respectively.

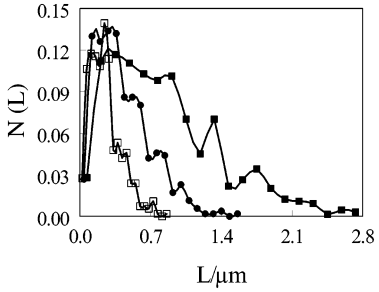

Figure 3. Length distribution functions of the nanofiber fractions 3 (■), 4 (●), and 5 (□), respectively.

TEM Results of the Nanofiber Fractions. The nanofibers fractions were prepared following the method described in the Experimental Section. Shown in parts a and b of Figure 2 are TEM images of fractions 1 and 4, respectively. The lengths of more than 500 nanofibers were measured manually for each fraction directly from such images at higher magnifications. Figure 3 gives results of such measurements for fractions 3, 4, and 5. Similar plots were obtained for fractions 1 and 2. The term $N(L_i)$ in Figure 3 is proportional to the probability

Table 3. Characteristics of the PS-*b*-PI Nanofiber Fractions

sample	TEM L_w (nm)	TEM L_n (nm)	M_w (g/mol)	R_G (nm)	l_p (nm)
F1	3110	1970	8.5×10^8	427	160
F2	1760	1210	4.9×10^8	347	225
F3	1190	840	3.7×10^8	280	280
F4	600	430	2.2×10^8	171	310
F5	340	250	1.2×10^8	117	920

of finding fibers with length between $(^1/_2)(L_i + L_{i-1})$ and $(^1/_2)(L_i + L_{i-1})$. Using the distribution data $N(L_i)$, we computed the number-average length, L_n, and weight-average length, L_w, of the fiber fractions with results shown in Table 3. Both L_w and L_n decreased with ultrasonication as expected. So did the polydispersity L_w/L_n of the fibers which was ~1.4 for all fractions.

Weight-Average M_w of the Nanofiber Fractions. The light scattering data were treated with

$$\frac{Kc}{\Delta R_\theta} = \frac{1}{M_w}[1 + (^1/_3)q^2{R_G}^2 - kq^4{R_G}^4 + ...] + 2A_2c \quad (1)$$

where c denotes nanofiber concentration in THF, ΔR_θ is the Rayleigh ratio, A_2 is the second virial coefficient, K is the optical constant of the system including terms such as the refractive index n_0 of the solvent, the laser wavelength λ, and the specific refractive index increment of the nanofiber etc., and k is a fitting constant. The term q is the scattering wave vector with magnitude given by

$$q = \frac{4\pi n_0}{\lambda}\sin(\theta/2) \quad (2)$$

where θ is the scattering angle. It should be born in mind that eq 1 is valid only at low scattering angles for which

$$qR_G/\sqrt{3} < 1 \quad (3)$$

where R_G denotes the z-average radius of gyration of the nanofibers.

Illustrated in Figure 4 is a Zimm plot for the light scattering data of F3 in the scattering angle range of 15 to 35°. Treating the scattering data with eq 4 yielded $M_w = 3.7 \times 10^8$ g/mol and $R_G = 280$ nm. The data of other fractions were treated similarly, with results shown in Table 3.

Plotted in Figure 5 are the M_w values thus obtained as a function of L_w determined from TEM. The data followed

$$M_w/(\text{g/mol}) = 3.2 \times 10^7 + M_U \times L_w \quad (4)$$

with the molar mass M_U of unit-length nanofibers given by 2.7×10^5 g/(mol·nm). The fact that M_w increased with nanofiber length and that M_U [g/(mol·nm)] agrees well with the M_U value of 2.53×10^5 g/(mol·nm) determined from the TEM radius and elemental analysis results suggests the validity of our light scattering M_w results.

Radius of Gyration R_G Data. The R_G values ranged from 117 nm for F5 to 427 nm for F1. For infinitely thin

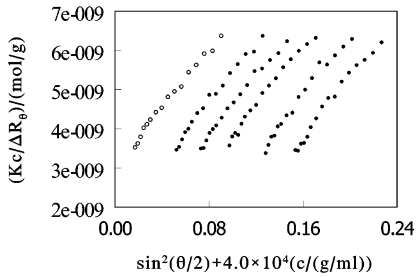

Figure 4. Zimm plot for the light scattering data of fraction 3 in the scattering angle range of 15 to 35°. The solid circles represent the experimental data. The hollow circles represent the extrapolated $Kc/\Delta R_{\theta|c\to 0}$ data.

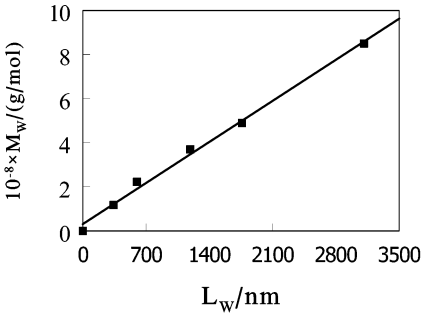

Figure 5. Plot of M_w determined from SLS as a function of weight-average length L_w for the different fractions.

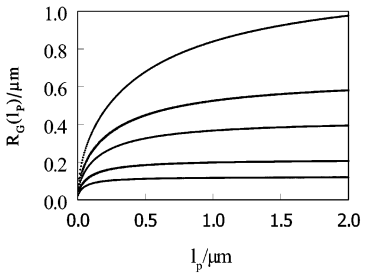

Figure 6. From top to bottom, plot of R_G calculated from eq 6 as a function of persistence length l_p for fractions 1, 2, 3, 4, and 5, respectively.

semiflexible wormlike chains, R_G is related to their contour length L and persistence l_p by[21]

$$R_G(L,l_p) = l_p\sqrt{L/3l_p - 1 + (2l_p/L)[1 - (l_p/L)(1 - e^{-(L/l_p)})]} \quad (5)$$

The R_G values determined from SLS is the z-average of $R_G(L_i/l_p)$:

$$R_G(l_p) = \frac{\sum_i N(L_i){L_i}^2 R_G(L_i/l_p)}{\sum_i N(L_i){L_i}^2} \quad (6)$$

where $N(L_i)$ is proportional to the population density of fibers with length L_i and has been evaluated from the TEM data such as those shown in Figure 3. Shown in Figure 6 are the $R_G(l_p)$ values, calculated from eq 6, plotted as a function of l_p for the different fractions. From this figure and the R_G values shown in Table 3, we obtained l_p values of 920, 310, 280, 225, and 160 nm for fractions 5, 4, 3, 2, and 1, respectively.

The decrease in l_p with nanofiber length can be at least partially explained by the fact that the finite

diameter d of the nanofibers contributed less to R_G with increasing nanofiber length. For a rigid uniform rod of length L with a rectangular cross section of side length a, R_G can be shown to be[22]

$$R_G = \sqrt{L^2 + 2a^2}/\sqrt{12} \quad (7)$$

A similar relation should apply to a cylindrical rod. In this case, the diameter d of the rod will replace a in eq 7. The flexibility of a rod will lead to further modification of eq 7 with the relative contribution of d to R_G increasing with increasing flexibility. Thus, the finite thickness of a rod increases R_G relative to that of an infinitely thin rod and this contribution increases with decreasing aspect ratio L/d and increasing nanofiber flexibility. For $L/d \approx 10$, the contribution is ~2% for rigid rods but is larger for semiflexible chains.

The positive contribution of d to R_G increases the resultant l_p values calculated from eq 6. This effect on l_p is especially pronounced for F5 not only for the fact it has the smallest aspect ratio L/d among the different fractions but also for the fact that the R_G value of 117 nm falls on the leveled-off region of the R_G-vs- l_p curve as shown in Figure 6. While $l_p = 910$ nm for $R_G = 117$ nm, the resultant l_p value decreases to 340 nm if R_G drops to 108 nm, for example. Fortunately, the R_G values for the other fractions fall in the region of the R_G-vs- l_p curve where R_G changed sensitively with l_p, and thus the l_p values for these fractions should be more accurate.

The decrease in l_p with increasing nanofiber length may also be an intrinsic property of the nanofibers. The longer nanofibers bend more, because kinks or defects are more likely to occur along their contour length. The persistence length is larger for the shorter fibers because fibers break more readily at the defect spots or kinks during ultrasonication. Further experiments such as viscosity measurements will be required to check on likeliness for this scenario to occur.

Last, we would like to sound the alarm for the reliability of the R_G data for F1. At $R_G = 427$ nm, $qR_G/\sqrt{3} = 1.0$ at $\theta = 16.7°$. The validity of eq 1 in treating the scattering data in the angle range of 12 and 30° was questionable and the R_G value needs to be interpreted with caution for this sample.

Despite the possible sources of error, we are confident in stating that the persistence length of the fibers should be ~200 nm. This is comparable with the value of ~400 nm we estimated before for polystyrene-*block*-poly(2-cinnamoyloxyethyl methacrylate) nanofibers[7c] and ~570 nm determined by Won et al.[23] for poly(ethylene oxide)-*block*-polyisoprene nanofibers but much larger than 0.9 to 1.4 nm determined for polystyrene chains.[24]

Scaling Relation for R_G. The accurate equation relating R_G and L for wormlike chains is eq 5. Meaningful scaling relations are obtained for such chains only in either the rigid rod limit where $L/l_p \rightarrow 0$ or the coil limit where $L/l_p \rightarrow \infty$. We proceeded to find the scaling relation for the fractions anyhow to reconfirm that the nanofibers were indeed semirigid on this length scale. Illustrated in Figure 7 is a plot of $\log(R_G/\text{nm})$ vs $\log(M_w/(\text{g/mol}))$ for the fractions. The exponent v obtained for the scaling relation

$$R_G \propto M_w^{\,v} \quad (8)$$

depended on the data included in the analysis. If only the more reliable R_G data for F2, F3, and F4 were used, v was found to be 0.88. The exponent reduced to 0.78 if data for F2, F3, F4, and F5 were used. It further reduced to 0.69 if all data were used. Regardless of the data treatment methods, the exponents obtained were all higher than 0.60 expected for polymer chains in a good solvent[11] but smaller than 1.00 expected for rigid rod chains, which suggests that the nanofibers were indeed semirigid on this length scale.

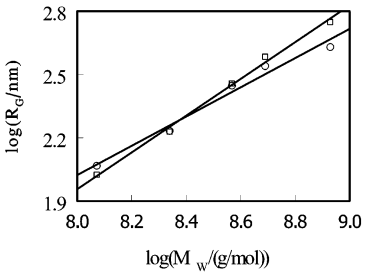

Figure 7. Plot of R_G vs M_w for the nanofiber fractions (○). Also shown are the R_G data (□) calculated from eq 6.

Also shown in Figure 7 are the $\log(R_G/\text{nm})$ data calculated using eq 6 assuming $l_p = 300$ nm for the different fractions. The scaling exponent v is 0.82 in this case.

IV. Conclusions

PS-*b*-PI nanofibers were prepared by stirring S_2Cl_2-treated PS-*b*-PI films in THF to separate and disperse the cross-linked PI cylindrical domains. Nanofibers with a relatively narrow molar mass distribution were obtained by collecting the fraction that remained dispersed at 11 000*g* but precipitated at 18 000*g*. This fraction was then ultrasonicated to yield four more fractions with even shorter lengths. The lengths of more than 500 fibers were measured from the TEM images for each fraction to yield the length distribution function $N(L)$, weight-average length L_w, and number-average length L_n. Each fraction was analyzed by static light scattering in the low scattering angle region to determine its weight-average molar mass M_w and radius of gyration R_G. The M_w values were found to increase with L_w linearly with M_U [g/(mol·nm)], which agreed with that determined from the TEM radius and elemental analysis results of the nanofibers. A quantitative analysis revealed that the persistence length of nanofibers decreased with nanofiber length and was typically ~200 nm.

Acknowledgment. The NSERC of Canada and Defense Research Development Canada are gratefully acknowledged for sponsoring this research.

References and Notes

(1) Price, P. *Pure Appl. Chem.* **1983**, *55*, 1563.
(2) Zhang, L. F.; Eisenberg, A. *Science* **1995**, *268*, 1728.
(3) Ding, J. F.; Liu, G. J.; Yang, M. L. *Polymer* **1997**, *38*, 5497.
(4) For block segregation patterns, see, for example: Bates, F. S. Fredrickson, G. H. *Phys. Today* **1999**, February, 32.
(5) (a) Tao, J.; Stewart, S.; Liu, G. J.; Yang, M. L. *Macromolecules* **1997**, *30*, 2738. (b) Stewart, S.; Liu, G. J. *Angew. Chem., Int. Ed.* **2000**, *39*, 340. (c) Liu, F. T.; Liu, G. J. *Macromolecules* **2001**, *34*, 1302.
(6) Won, Y.-Y.; Davis, H. T.; Bates, F. S. *Science* **1999**, *283*, 960.
(7) (a) Liu, G. J.; Qiao, L.; Guo, A. *Macromolecules* **1996**, *29*, 5508. (b) Liu, G. J. *Adv. Mater.* **1997**, *9*, 437. (c) Liu, G. J.; Ding, J.; Qiao, L.; Guo, A.; Gleeson, J. T.; Dymov, B.; Hashimoto, T.; Saijo, K. *Chem.—Eur. J.* **1999**, *5*, 2740.

(8) (a) Massey, J.; Power, K. N.; Manners, I.; Winnik, M. A. *J. Am. Chem. Soc.* **1998**, *120*, 9533. (b) Massey, J. A.; Temple, K.; Cao, L.; Rharbi, Y.; Raez, J.; Winnik, M. A.; Manners, I. *J. Am. Chem. Soc.* **2000**, *122*, 11577.
(9) (a) Yan, X. H.; Liu, G. J.; Liu, F. T.; Tang, B. Z.; Peng, H.; Pakhomov, A. B.; Wong, C. Y. *Angew. Chem., Int. Ed.* **2001**, *40*, 3593. (b) Yan, X. H.; Liu, G. J.; Liu, F. T. *Macromolecules* **2001**, *34*, 9112.
(10) Templin, M.; Franck, A.; DuChesne, A.; Leist, H.; Zhang, Y. M.; Ulrich, R.; Schadler, V.; Wiesner, U. *Science* **1997**, *278*, 5344.
(11) Liu, G. J.; Yan, X. H.; Qiu, X. P.; Li, Z. *Macromolecules* **2002**, *35*, 7742.
(12) De Gennes, P.-G. *Scaling Concepts in Polymer Physics*; Cornell University Press: Ithaca, NY, 1979.
(13) See, for example: (a) Cirkel, P. A.; Koper, G. J. M. *Langmuir* **1998**, *14*, 7095. (b) Pedersen, J. S.; Egelhaaf, S. U.; Schurtenberger, P. *J. Phys. Chem.* **1995**, *99*, 1299. (c) Jerke, G.; Pedersen, J. S.; Egelhaaf, S. U.; Schurtenberger, P. *Phys. Rev.* **1997**, *56*, 5772.
(14) Cates, M. E.; Candau, S. J. *J. Phys.: Condens. Matter* **1990**, *267*, 6869.
(15) Morton, M. *Anionic Polymerization: Principles and Practice*; Academic Press: New York, 1983.
(16) Ding, J. F.; Liu, G. J. *Macromolecules* **1999**, *32*, 8413.
(17) Ishizu, K.; Onen, A. *J. Polym. Sci.: A: Polym. Chem.* **1989**, *27*, 3721.
(18) Breiner, U.; Krappe, U.; Abetz, V.; Stadler, R. *Macromol. Chem. Phys.* **1997**, *198*, 1051.
(19) Yan, X. H.; Liu, F. T.; Li, Z.; Liu, G. J. *Macromolecules* **2001**, *34*, 9112.
(20) Khandpur, A. K.; Forster, S.; Bates, F. S.; Hamley, I. W.; Ryan, A. J.; Bras, W.; Almdal, K.; Mortensen, K. *Macromolecules* **1995**, *28*, 8796.
(21) Benoit, H.; Doty, P. *J. Phys. Chem.* **1953**, *57*, 958.
(22) This was derived directly from the definition of R_G. We used the center of mass of the rod as the origin of a Cartesian coordinate system. The probability density for finding mass elements between $-(a/2) \le x \le a/2$, $-(a/2) \le y \le a/2$, and $-(L/2) \le z \le L/2$, is equal to $1/(a^2L)$. The distance between point (x, y, z) and the center of mass is $\sqrt{x^2+y^2+z^2}$.
(23) Won, Y.-Y.; Davis, H. T.; Bates, F. S.; Agamalian, M.; Wignall, G. D. *J. Phys. Chem. B.* **2000**, *104*, 7134.
(24) (a) Pedersen, J. S.; Schurtenberger, P. *Macromolecules* **1996**, *29*, 7602. (b) Aharoni, S. M. *Macromolecules* **1983**, *16*, 1722.

MA021021B